Structural Investigations of AMS-n Mesoporous Materials by Transmission Electron Microscopy

Alfonso E. Garcia-Bennett* and Osamu Terasaki

Structural Chemistry, Arrhenius Laboratory, Stockholm University, S-10691 Stockholm, Sweden

Shunai Che*

Department of Chemistry, School of Chemistry and Chemical Technology, Shanghai Jiao Tong University, 800 Dongchuan Road, Shanghai, 200240, P. R. China

Takashi Tatsumi

Division of Materials Science & Chemical Engineering, Faculty of Engineering, Yokohama National University, 79-5 Tokiwadai, Yokohama 240-8501, Japan

Received October 27, 2003. Revised Manuscript Received December 1, 2003

A novel synthesis route for mesoporous silicates using anionic surfactants has been recently reported. It was advanced that materials synthesized using anionic surfactants and aminosilane groups as co-structure directing agents led to the synthesis of highly ordered, novel mesoporous materials with unprecedented structural properties. Here we present an in-depth high-resolution transmission electron microscopy (HRTEM) investigation on the structural characteristics of these novel mesoporous solids denoted AMS-n (anionic mesoporous silicas). These materials show increased order in comparison with conventional mesoporous structures as a result of the long-range periodicity of structural modulations. Structural defects formed in these materials are investigated using electron diffraction (ED) and Fourier transform (FT) diffractograms. In addition we present a new cubic mesostructure AMS-8 (space group $Fd\bar{3}m$). These new materials show promising new pore connectivities and morphologies making them ideal for applications ranging from catalysts' supports to gas separation, and from nanodevices to drug delivery.

Introduction

The initial mechanism for the synthesis of mesoporous materials,[1] involving the use of cationic surfactants as structure-directing agent, has now expanded to include nonionic polymer and anionic surfactants.[2] Variations in the structure-directing agent and synthesis conditions have led to the formation of mesoporous materials with a large variety of pore sizes (from 18 to 100 Å without the use of additives), connectivities, morphologies, and structures; for example the 3-dimensionally (3d) connected caged cubic structure SBA-1 (space group $Pm\bar{3}n$),[3] the 3d-bicontinuous cubic structure of MCM-48 and its large-pore equivalent FDU-5 ($Ia\bar{3}d$),[4] the 2d-hexagonal structure of SBA-15 ($p6mm$) analogous to MCM-41,[5] the wormhole structured HMS-n materials,[6] and the intergrowth structures of SBA-2 and SBA-12.[7] Besides finding applications in petroleum cracking, mesoporous materials have shown catalytic activity in many reactions such as oxidation, acid catalysis, and hydroxylation.[2,8] In addition, applications as nano-reactors, in optical devices, and as "drug-delivery" supports are showing promising results.[9,10,11]

The formation mechanism of mesoporous silicates has been previously discussed on the basis of electrostatic interactions, denoted S^+I^- (alkaline pH 9−14 conditions) and $S^+X^-I^+$(pH ∼1) templating pathways; where S

* To whom correspondence should be addressed. E-mail: alf@struc.su.se (A.E. Garcia-Bennett) and chesa@sjtu.edu.cn (S.Che).

(1) Kresge, C. T.; Leonowicz, M. E.; Roth, W. J.; Vartulli, J. C.; Beck, J. S. *Nature* **1992**, *359*, 710.

(2) Inagaki, S.; Fukushima Y.; Kuroda, K. *Chem. Commun.* **1993**, *8*, 680. Huo, Q.; Margolese, D. I.; Ciesla, U.; Feng, P. Y.; Gier, T. E.; Sieger, P.; Leon, R.; Petroff, P. M.; Schüth, F.; Stucky, G. D. *Nature* **1994**, *368*, 317. Corma, A. *Chem. Rev.* **1997**, *97*, 2373.

(3) Sakamoto, Y.; Kaneda, M.; Terasaki, O.; Zhao, D. Y.; Kim, J. M.; Stucky, G.; Shin, H. J.; Ryoo, R. *Nature* **2000**, *408*, 449. Carlsson, A.; Kaneda, M.; Sakamoto, Y.; Terasaki, O.; Ryoo, R.; Joo, H. *J. Electron Microscopy* **1999**, *48*, 795.

(4) Kaneda, M.; Tsubakiyama, T.; Carlsson, A.; Sakamoto, Y.; Ohsuna, T.; Terasaki, O.; Joo, S. H.; Ryoo, R. *J. Phys. Chem. B.* **2002**, *106*, 1256. Liu, X.; Tian, B.; Yu, C.; Gao, F.; Xie, S.; Tu, B.; Che, R.; Peng, L.; Zhao, D. Y. *Angew. Chem., Int. Ed.* **2002**, *41*, 3876.

(5) Zhao, D. Y.; Feng, J.; Huo, Q.; Melosh, N.; Fredrickson, G. H.; Chmelka B. F.; Stucky G. D. *Science* **1998**, *279*, 548.

(6) Tanev, P. T.; Pinnavaia, T. J. *Science* **1995**, *865*, 267. Bagshaw, S. A.; Prouzet, E.; Pinnavaia, T. J. *Science* **1995**, *269*, 1242. Tanev, P. T.; Pinnavaia, T. J. *Chem. Mater.* **1996**, *8*, 2068.

(7) Huo, Q.; Margolese, D. I.; Ciesla, U.; Demuth, D. G.; Feng, P.; Gier, T. E.; Sieger, P.; Firouzi, A.; Chmelka, B.; Schüth, F.; Stucky, G. D. *Chem. Mater.* **1994**, *6*, 1176. Zhao, D.; Hou, Q.; Feng, J.; Chmelka, B. F.; Stucky, G. D. *J. Am. Chem. Soc.* **1998**, *120*, 6024.

(8) Van Bekkum, H.; Hoefnagel, A. J. *Stud. Surf. Sci. Catal.* **1994**, *83*, 397. Kageyama, K.; Tamazawa J.; Aida, T. *Science* **1999**, *285*, 2113.

(9) Huang, M. H.; Choudrey, A.; Yang, P. *Chem. Commun.* **2000**, 1063.

(10) Marlow, F.; McGehee, M. D.; Zhao, D.; Chmelka B. F.; Stucky, G. D. *Adv. Mater.* **1999**, *11*, 632. Yang, P. D.; Wirnsberger, G.; Huang, H. C.; Cordero, S. R.; McGehee, M. D.; Scott, B.; Deng, T.; Whitesides, G. M.; Chmelka, B. F.; Buratto S. K.; Stucky, G. D. *Science* **2000**, *287*, 465.

(11) Munoz, B.; Ramila, A.; Perez-Pariente, J.; Diaz. I.; Vallet-Regi, M. *Chem. Mater.* **2003**, *15*, 500.

10.1021/cm035074z CCC: $27.50
Published on Web 02/03/2004

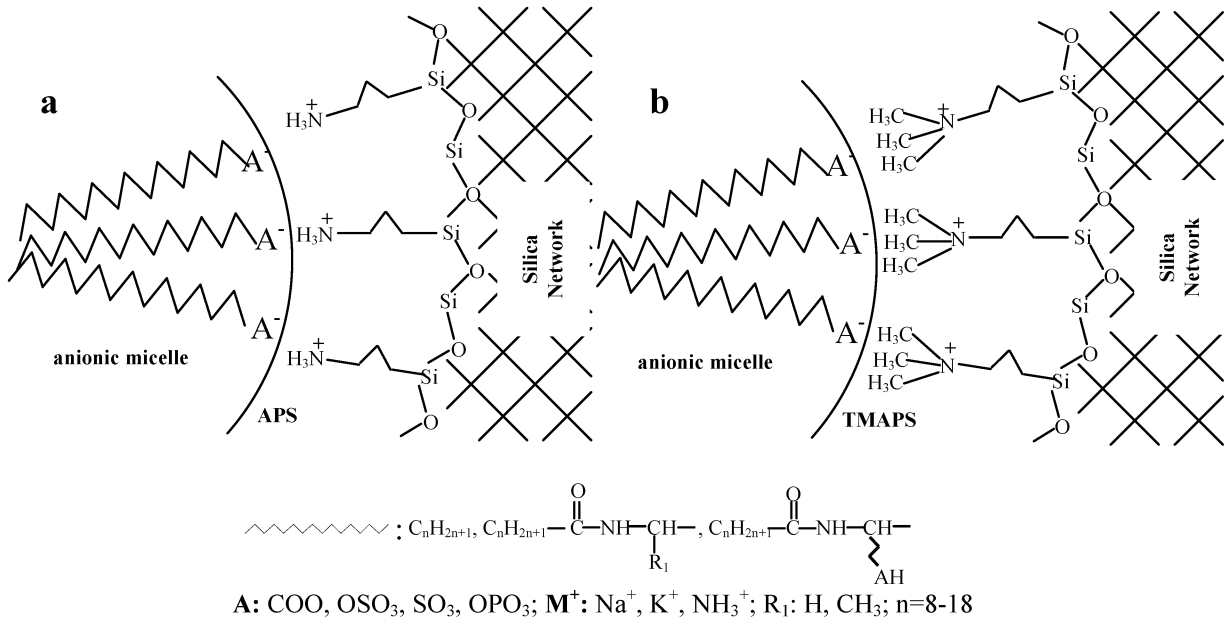

Figure 1. Schematic representation of species involved in the synthesis of AMS-n materials with 3-aminopropyltrimethoxysilane APS (a), and *N*-trimethoxysilylpropyl-*N*,*N*,*N*-trimethylamonium chloride TMAPS (b) as co-structure-directing agents.

denotes the surfactant, I is the inorganic phase, and X is the mediating surfactant counterion. The S^0I^0 templating pathway has been also proposed to explain the generation of HMS-n type mesoporous solids. This involves synthesis carried out at neutral conditions using neutral organic amines or nonionic oligomeric surfactants (S^0) as templates. It should be noted that at such conditions both the inorganic and organic species are not strictly neutral. Hydrogen bonding may play an important role for these partially charged inorganic and/or organic species.

The use of anionic surfactants to direct the self-assembly of cationic and anionic metal oxide (M^+) species through S^-I^+ and $S^-M^+I^-$ metal counterion mediated ion pairs has been reported previously, but these preparations have resulted mainly in lamellar and disordered structures.[12] With an aim to increase the interaction between the silicate species and the structure-directing agent, Che et al. have successfully prepared highly ordered mesoporous materials using anionic surfactants *N*-acylalanine (C_nAla(A,S) where C_n = C_nH_{2n+1}, A = free acid, and S = sodium salt; glycine (C_nGly(A,S)); and *N*-acyl-glutamic acid (C_nGlu(A,S)),[13] in the presence of CSDA *N*-trimethoxysilylpropyl-*N*,*N*,*N*-trimethylamonium chloride (TMAPS) and 3-aminopropyltrimethoxysilane (APS) under alkaline conditions. This family of materials has been named AMS-n (anionic surfactant templated mesoporous silica). Here, the mechanism is thought to be controlled by the electrostatic interaction between the negatively charged carboxylic headgroup of the anionic surfactant and the amine group of the organoalkoxysilane. Condensation occurs preferentially at the alkoxysilane sites in APS and TMAPS to onset the formation of the silicate framework. The species involved are schematically shown in Figure 1. This new templating pathway, termed here $S^-\bar{N}^+ \sim \bar{I}$, where $\bar{N}^+ \sim \bar{I}$ represents the positively and negatively charged amine and silane groups, respectively, allows for the synthesis of mesoporous structures using widely available anionic surfactants and opens up new synthetic and structural possibilities.

The amorphous nature of mesoporous "cavity-crystals" prevents structural elucidation using X-ray diffraction (XRD) techniques because of the low number of observed reflections. This makes the unambiguous solution of the 3d-structures by XRD alone extremely difficult. HRTEM structural investigations must be conducted if one is to elucidate the internal pore structure, connectivity, and shape of pores. These characteristics must be known to fully appreciate the potential of mesoporous materials. Recently, it has been shown that structural solutions can be derived unambiguously by electron microscopy and electron crystallography.[3] The 3d-structures of MCM-48 ($Ia\bar{3}d$), SBA-1 ($Pm\bar{3}n$), SBA-6 ($Pm\bar{3}n$), SBA-12 ($Fm\bar{3}m$), SBA-16 ($Im\bar{3}m$), and the carbon-replica CMK-type materials have been so far investigated in this way. [3−6]

Structural speculations based on XRD evidence and initial studies by HRTEM have allowed Che et al. to suggest the formation of 2d-/3d-hexagonal (AMS-3 and AMS-1, respectively), 3d-cubic (AMS-2 and AMS-4), and lamellar (AMS-5) mesophases through variations in anionic surfactant, co-structure-directing agent (CSDA), and synthetic conditions.[9] This work alone demonstrates the versatility of this templating pathway. In addition periodic structural modulations were observed. Defects in mesoporous solids are common and have been studied by HRTEM on the intergrowth structures SBA-2 and SBA-12 where hexagonal close-packed (*hcp*) and cubic close-packed (*ccp*) stacking faults are clearly defined.[10−12] However, in these systems, the abundance of one co-structure over the other is difficult to control, and efforts to form the single 3d-hexagonal SBA-2 and SBA-12 phases have been futile, so far, when using conditions

(12) Antonelli, D. M.; Ying, J. Y. *Angew. Chem., Int. Ed. Engl.* **1996**, *35*, 426. Wong, M. S.; Ying, J. Y. *Chem. Mater.* **1998**, *10*, 2067.

(13) Che, S.; Garcia-Bennett, A. E.; Yokoi, T.; Sakamoto, K.; Kunieda, H.; Terasaki, O.; Tatsumi, T. *Nature Materials*, advanced online publication, November **2003**.

Table 1. Synthesis Conditions for the Preparation of Mesoporous Solids AMS-1−8

mesophase	surfactant, CSDA[a]	surfactant conctn. (%)	CSDA/surf.	Si/surf.	pH	temp. (°C)	time (days)
AMS-1	C_{14}GluS, TMAPS	1.0	2.0	12.0	8.9	100	3
AMS-2	C_{12}GluA, APS	1.0	2.5	21.0	8.7	100	2
AMS-3	C_{16}AS, TMAPS	1.0	1.0	10.0	9.2	60	1
AMS-4	C_{12}AlaA, APS	1.0	0.75	8.3	5.2	60	1
AMS-5	C_{12}AlaA, APS	1.0	1	4	9.4	60	1
AMS-6	C_{12}AlaA, APS	0.7	0.75	6.75	5.0	60	1
AMS-7	C_{14}GluSA, TMAPS	1.0	1.5	16.5	9.0	100	1
AMS-8	C_{12}GlyS, TMAPS	1.0	1.0	10.0	8.8	100	4

[a] A = Free acid, S = sodium salt, Glu = L-glutamic acid, Ala = L-alanine, Gly = glycine, and C_n= C_nH_{2n+1} = $C_{12}H_{23}O$, *N*-lauroyl; $C_{14}H_{27}O$, *N*-myristoyl; $C_{16}H_{31}O$, *N*-palmitoryl.

similar to those of the original SBA-2 synthesis (under alkaline, room-temperature conditions). The formation of a 3d-hexagonal mesophase using the gemini surfactant C16-3-1 was reported recently, under acid conditions and at low temperatures.[12] Mesoporous solids AMS-2 and AMS-4 show periodic structural modulations, suggesting that this is a property inherent of the micelle structure. The possibility of formation of two distinct micellar species has also been suggested. The morphology of 3d-hexagonal AMS-1 synthesized with anionic surfactant *N*-acyl-glutamic acid and TMAPS as CSDA shows also a puzzling surface structure where a 1d porous network is clearly visible growing surrounding the ordered 3d-structure. We also present here the synthesis and characterization of related mesophases AMS-6, 7, and 8. HRTEM investigations conducted on these materials will be discussed with an aim to gain insight into the formation mechanism and to confirm the structural characteristics of this new and promising mesoporous family.

Experimental Section

The synthesis of mesoporous materials AMS-1−5 has already been reported.[13] Briefly, in a typical synthesis a mixture of TEOS and CSDA TMAPS/APS (50% in methanol) was added to a solution of the desired anionic surfactant in deionized water with stirring at 60 °C. After the mixture was stirred for 24 h, the mesostructured product formed was cured at 100 °C for 1−3 days. The products were filtered and dried at 333 K. AMS-n silicas can be synthesized with 0.5−5 wt % surfactants, 1−2 molar ratio of quaternary aminosilane/anionic salt surfactant, and 2−6 molar ratio of primary aminosilane/glutamic acid using a wide pH range (5−11). All of the anionic surfactants and the organics of the co-structure-directing agents can be removed by calcination at 600 °C for 6 h under flowing N_2/O_2. For the purpose of obtaining amino-functionalized mesoporous silica, the surfactants were removed by exhaustive solid−liquid extraction using 10 vol. % H_2O ethanol solution at boiling point overnight. Mesoporous materials AMS-6 and 8 were synthesized in the same way. The synthesis of AMS-7 differs in that the additive tetrapropylammonium bromide (TPABr, APS/TPABr = 1) was added to the synthesis gel prior to addition of TEOS. TPABr and APS react with the carboxylate sodium salt and the cabolyxilic acid groups of the anionic surfactant, respectively. Table 1 summarizes the molar composition of reaction gels and the synthesis conditions employed in the synthesis of AMS-1−8.

XRD patterns were recorded on an MX Labo powder diffractometer equipped with Cu Kα radiation (40 kV, 20 mA) at the rate of 1.0 deg/min over the range of 1.5−10.0° (2θ). The N_2 adsorption−desorption isotherms were measured at −196 °C on a Belsorp 28SA sorptionmeter.

Transmission electron microscopy (TEM) was conducted with a JEOL-3010 microscope, operating at 300 kV (Cs 0.6 mm, resolution 1.7 Å). Images were recorded using a CCD-camera (model KeenView, SIS analysis, size 1024 × 1024, pixel size 23.5 × 23.5 μm) at 30 000−100 000× magnification using low-dose conditions. A typical HRTEM image observed from AMS-n and its corresponding Fourier transform (FT) is shown in Figure 3a. FT diffractograms were conducted using Digital Micrograph software (Gatan). Lattice angle calculations were conducted using the software Ucalc.[14]

Results and Discussion

For simplicity each structure is discussed in turn in the text that follows. XRD patterns of calcined samples of AMS-n mesoporous materials are shown in Figure 2 and structural characteristics and porosity data of AMS-n materials are summarized in Table 2. The discussion centers on the structural characterization of AMS-type materials followed by a brief summary of the synthetic implications derived from the study. The lamellar structure of AMS-5 has been discussed previously so it has been omitted from this discussion.[13]

AMS-1. Mesoporous material AMS-1 was synthesized by the use of C_{14}GluS and TMAPS as co-structure-directing agents. The XRD pattern for this sample shows sharp intensities between 1 and 5° 2θ and can be indexed on the basis of a hexagonal unit cell (a = 54.4 Å and c = 88.2 Å) with a c/a ratio of unit cell 1.629 Å. Figure 3 shows TEM images recorded with incidence beam parallel to the $[001]_h$ orientation of calcined AMS-1 synthesized after curing for 1 day and with a Si/surfactant ratio = 12. This sample is composed of spherical/cylindrical particles of sizes ranging from 10 to 100 nm. FT diffractograms (inset in Figure 3a) taken from thin sections of the image show streaking of diffraction spots that can be attributed to the small domains exhibited by the particle and to a large amount of structural defects. A disordered 1-dimensional (1d)

(14) Ucalc software, available from Prof. T. Ohsuna at *http://www-lab.imr.tohoku.ac.jp/ohsuna/* or ohsuna@struc.su.se.

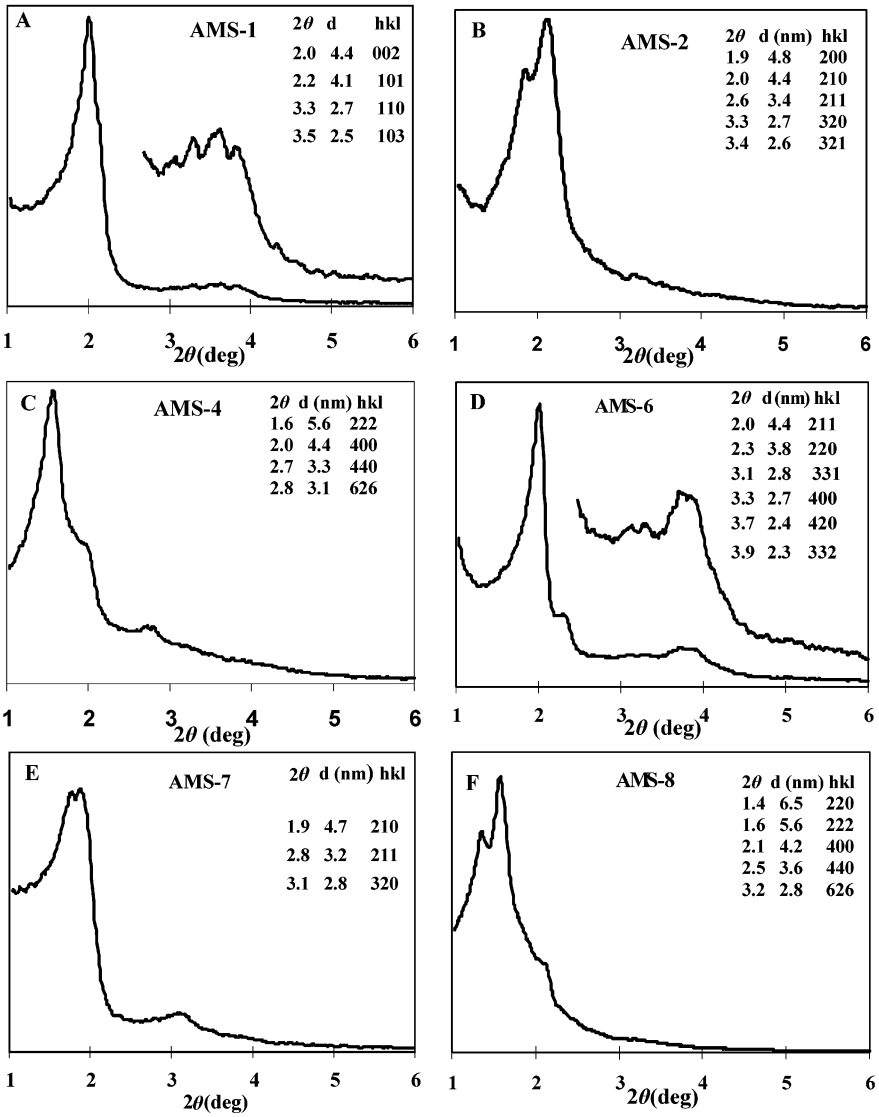

Figure 2. XRD patterns of calcined mesoporous materials AMS-1, -2, -4, -6, -7, and -8. Tables shown as insets show indexed reflections for observed peaks. The XRD pattern of calcined AMS-3 is shown in the Supporting Information.

Table 2. Structural Data Derived from XRD and N_2 Isotherms for AMS-n Materials

structure	unit cell[a] (Å)	surface area (m^2g^{-1})[b]	pore volume ($cm^3\ g^{-1}$)	pore diameter[c] (Å)
AMS-1 (3d-hexagonal)	$a = 54.4$ $c = 88.2$	501	0.316	23
AMS-2 (3d-cubic)	96.1	963	0.692	28[d]
AMS-3 (2d-hexagonal)	81.9	387	0.510	62
AMS-4 (3d-cubic)	183.9	760	0.794	40
AMS-6 (3d-cubic)	107.7	667	0.651	32
AMS-7 (3d-disordered)	100.0	301	0.328	23[d]
AMS-8 (3d-cubic)	183.4	271	0.220	23[d]

[a] Calculated from the XRD patterns. [b] Calculated by the BET method. [c] Calculated from the adsorption branch of the N_2 isotherm using the BJH method. [d] These values are quoted for comparison only, as the BJH model is not valid for pore sizes below 30 Å.

channel domain ranging in thickness from 2 to 10 nm surrounds each particle. The "central porous structure" is accessible, however, to the external surface through this disordered domain (highlighted in Figure 3b) although the material shows a lower surface area than other mesoporous materials synthesized with anionic surfactants in this study, suggesting that the level of connectivity between external and internal surfaces may be decreased as a result of formation of the 1d-channel mesophase.

AMS-2. The XRD pattern of calcined AMS-2 mesoporous silicas synthesized by using C_{12}GluA and APS is shown in Figure 2b. This sample shows two well-resolved, sharp XRD diffraction peaks in the region of $2\theta = 1.5-3.0°$. The ratio of d spacing of the two first peaks is close to $\sqrt{5}/2$; these can be indexed as the 200 and 210 reflections ($a = 96.1$ Å), based on a cubic lattice. HRTEM images recorded along the [100] and [210] zone axis (Figure 4a and b, respectively) reveal clear large ordered regions indicating that the crystal is a well-ordered mesostructure. It is possible to index FT diffractograms taken along thin areas (shown as insets) on the basis of a 3d-cubic unit cell with $Pm\bar{3}n$ space-group and extinction rules are satisfied. However, it is clear from Figure 4a that neighboring unit cells are

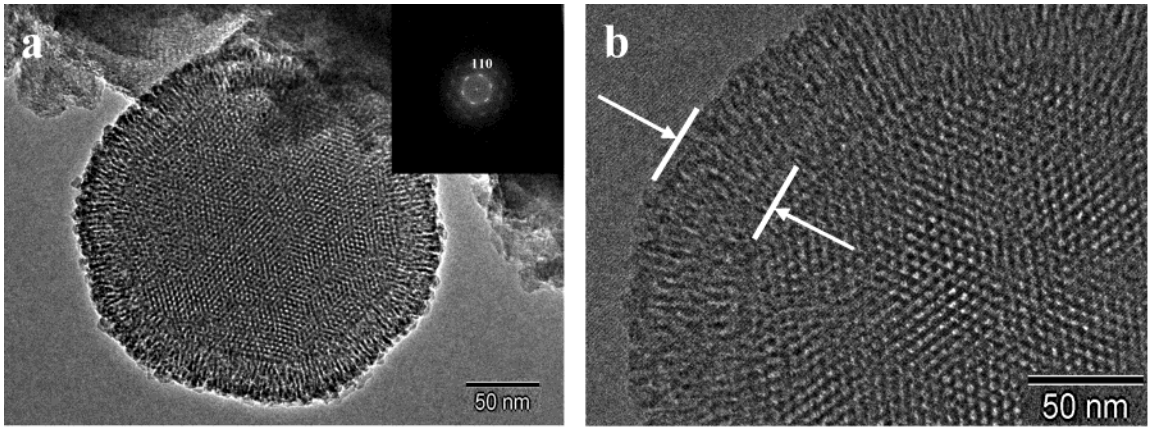

Figure 3. HRTEM image of calcined AMS-1 mesoporous material recorded along the [001] orientation. Flat-shaped cylindrical particles are clearly observed throughout the sample. Although the sample was crashed in a pestle and mortar before deposition on a copper grid, no broken particles could be found, suggesting a sharp particle size and a flat-shaped morphology. The inset in Figure 3b highlights the 1d disordered porous system that surrounds each particle. This growth feature can also be observed in other AMS-type materials despite their larger particle size.

displaced by a half (these have been highlighted in the image) forming an antiphase boundary. These periodic displacements are represented by clear electron density modulations in the FT diffractograms. No extra reflections arising from this are observed on the XRD pattern of calcined AMS-2 (Figure 2b). On this basis, another cubic structure with lattice constant a_2 can be assigned. We can presume that these are formed with stabilization mechanisms different from that for the SBA-1 mesophase prepared using conventional cationic surfactants. The unit cell constants a_1 and a_2 are 93 and 142 Å, respectively (the unit cells are outlined in Figure 4a). The cubic unit cell parameter calculated from images recorded along the [210] direction (a = 89.0 Å) is in reasonable agreement with the XRD calculated unit cell value a = 96.1 Å; the difference can be attributed to the modulated structure and inevitable experimental error. This indicates that modulations are present throughout the whole crystal and not in isolated domains. In addition, stacking faults can also be observed in Figure 4a. Some of these have been highlighted on the image. It is important to note that although this material is related, in spacegroup symmetry, to the mesocaged solid SBA-1, the expected pore connectivities between cages and internal surface will be considerably different as a result of the abundant modulations and defects. Sakamoto et al. have described the bimodal arrangement of cages and connecting pores in SBA-1 to be of type A_3B. From this study, in the "modulation-free" SBA-1 structure, cages perpendicular to the [100] orientation are known to form straight channels. This is not the case of AMS-2 because the cages perpendicular to the [100] orientation will have a zigzag arrangement. Further studies of the pore connectivity of this material resulting from its structural modulations are being conducted. Furthermore, the presence of a similar 1d porous system can also be clearly observed surrounding AMS-2 particles, where the growth of the less ordered phase occurs epitaxially (highlighted in Figure 4a).

AMS-3. The XRD pattern of calcined AMS-3 mesoporous material synthesized using anionic surfactant C_{16}-AS (shown as Supporting Information) can be indexed on the basis of a hexagonal unit cell, and TEM images prove that AMS-3 is indeed similar to hexagonal MCM-41. Unit cells calculated by HRTEM and XRD data (a = 93.6 and 92.4 Å, respectively) agree within experimental error, and no structural modulations or defects were observed in this mesoporous material. The 2d-hexagonal structure of AMS-3 was synthesized using a variety of anionic surfactants. Figure 5 shows TEM images recorded on calcined AMS-3, showing pores parallel (Figure 5a) and perpendicular (Figure 5b) to the incident electron beam.

AMS-4. Figure 2c shows the XRD pattern of calcined AMS-4. Sharp mesoporous peaks can be observed. HRTEM images of calcined AMS-4 mesoporous solid synthesized with C_{12}−AlaA anionic surfactant and APS as CSDA are shown in Figure 6. The presence of a plane containing 6-fold symmetry is clearly observed in Figure 6a, hence cubic or hexagonal crystal classes can be assumed. From consideration of theoretical and calculated tilting angles between lattice planes and related reflections, a hexagonal crystal lattice with unit cell parameters a = 50.8 Å and c = 80.2 Å was selected. Other TEM images recorded along the high-symmetry zone axis confirm the presence of a single hexagonal phase (Figure 6b), however the coexistence of a cubic structure cannot be ruled out. Figure 6c shows an HRTEM image recorded along a single stacking fault showing clear two separate domains with ABABAB... and ABCABC... stacking sequences associated with hexagonal and cubic structures, respectively. This is not unexpected as the *hcp* and *ccp* stacking faults have been observed previously in mesoporous materials,[15,16,17] and in zeolites alike.[18] FT Diffractograms taken on either side of the stacking fault (shown as insets, Φ and θ) confirm the presence of a cubic F type structure with a = 70.8 Å. In addition, a clear relation between the $[210]_h$ and $[110]_c$ orientations is observed, where $d_{(002)h} = d_{(220)c}$ suggesting that the growth mechanisms involved in the

(15) Hunter, H. M. A.; Garcia-Bennett, A. E.; Shannon, I. J.; Zhou, W.; Wright, P. A. *J. Mater. Chem.* **2002**, *12*, 20.
(16) Sakamoto, Y.; Diaz, I.; Terasaki, O.; Zhao, D.; Perez-Pariente, J.; Kim J. M.; Stucky, G. D. *J. Phys. Chem. B.* **2002**, *106*, 3118.
(17) Garcia-Bennett, A. E.; Williamson, S.; Wright, P. A.; Shannon, I. J. *J. Mater. Chem.* **2002**, *12*, 3533.
(18) Anderson, M.; Pachis, K. S.; Prebin, F.; Carr, S. W.; Terasaki, O.; Ohsuna, T.; Alfredsson, V. *Chem. Commun.* **1992**, *218*, 61.

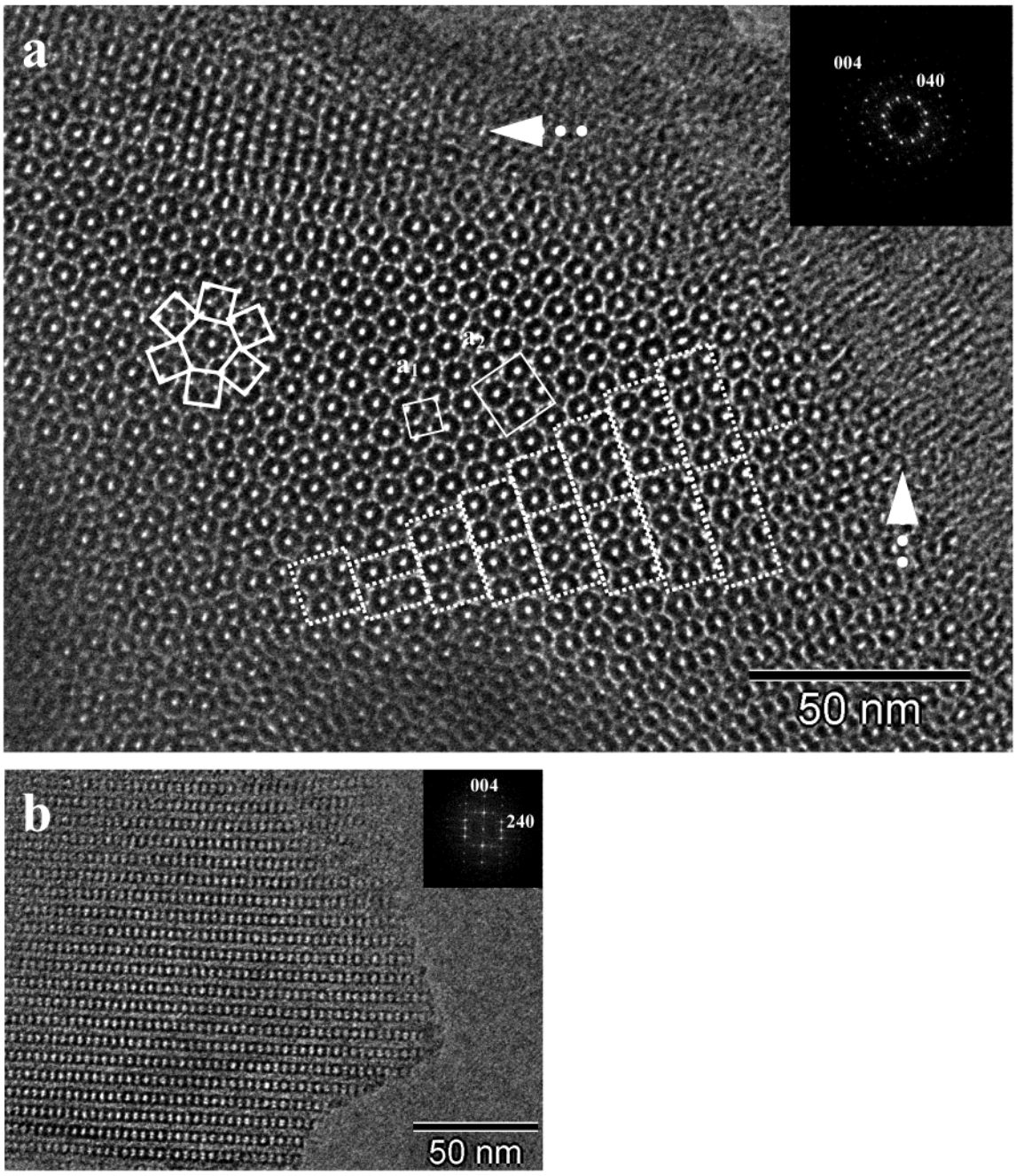

Figure 4. HRTEM images recorded along the [100] and [210] zone axis of calcined AMS-2 (a and b, respectively) with their corresponding FT diffractograms (insets). Figure 4a shows the presence of a typical 1d amorphous domain growing epitaxially similar to that observed previously in AMS-1 (arrows), an antiphase domain boundary (dotted line), and two possible cubic unit cells (a_1 and a_2). In addition, a more complex defect is highlighted for its 4- and 6-member nearest neighbor motive.

formation of the cubic and hexagonal structures are closely related. A further cubic phase has also been identified in the bulk AMS-4 sample. Figure 6d shows an image recorded with incidence direction [011] based on a cubic face-centered structure with $a = 183.9$ Å. Such contrast patterns have never been reported in mesoporous materials previously, suggesting that this indeed may be a new mesophase. Although there are clear systematic extinctions, the complex mixture of phases in this material makes it extremely hard to elucidate the structure even by HRTEM. The formation of three different mesoporous phases under stirring conditions is evidence for the formation of at least two different micellar species. Further structural and synthetic investigations are being conducted to determine the different proportions of phases in this sample. From the XRD pattern we can assume that the face-centered cubic phase with $a = 183.9$ Å is present in larger proportions in the bulk material, because the XRD pattern of calcined AMS-4 can be indexed on the basis of a cubic face-centered unit cell with $a = 185.3$ Å, a value which agrees well with the TEM-derived unit cell parameter.

AMS-6. Figure 7 shows TEM images recorded on calcined samples of AMS-6 synthesized with C_{12}AlaA anionic surfactant and APS as CSDA, after curing for 2 days and with a TEOS/surfactant ratio = 6.75. The morphology of the sample is composed of thin spherical particles of size 10−80 nm. These are similar to those reported above for sample AMS-1. Images show contrast

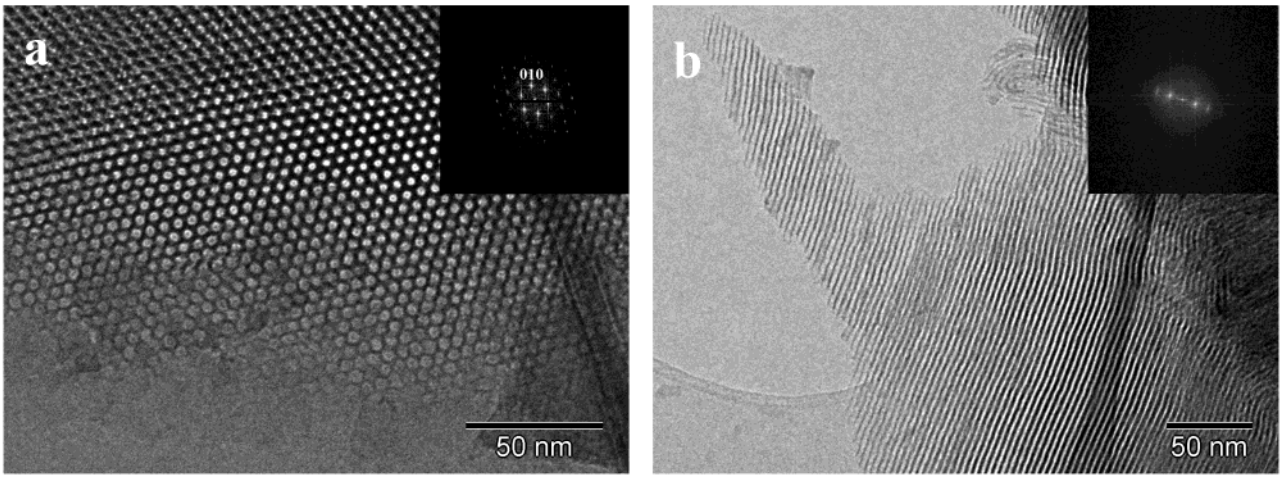

Figure 5. TEM images recorded on calcined AMS-3, showing pores parallel (a) and perpendicular (b) to the electron beam.

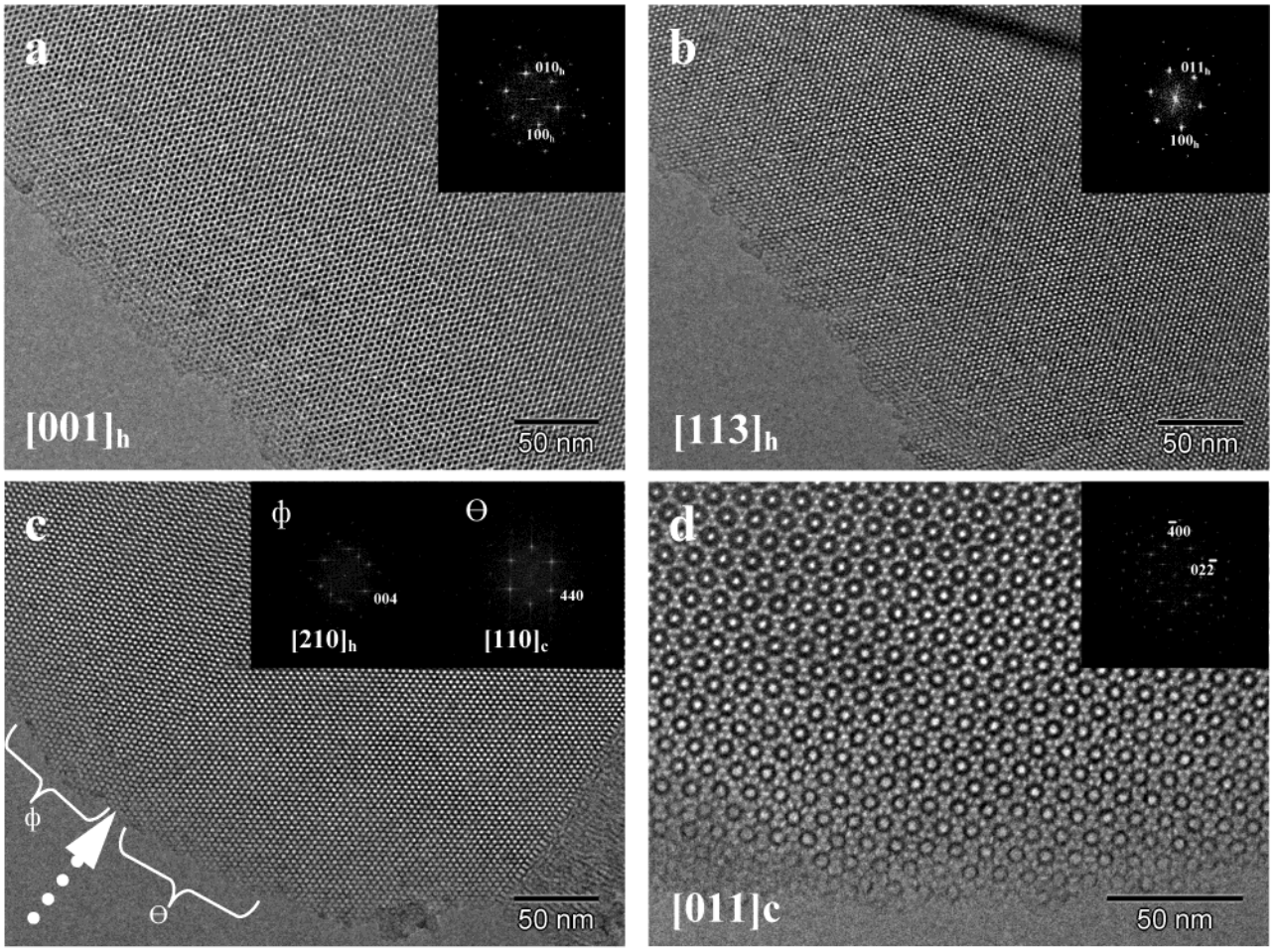

Figure 6. HRTEM images recorded along high-symmetry axis of calcined hexagonal/cubic intergrowth structure AMS-4 synthesized with surfactant C_{12}AlaA and APS as CSDA. HRTEM images recorded along the [001] (a) and [113] (b) zone axis based on hexagonal lattice. Beautiful periodicity over large areas is clearly observed. Figure 6c shows the presence of a single stacking fault showing ABABAB... and ABCABC... type stacking, associated with *hcp* and *ccp* structures, respectively. An HRTEM image recorded along the [011] direction of a further cubic phase is shown in Figure 6d.

patterns consistent with 3d-bicontinuous cubic ($Ia\bar{3}d$) mesoporous materials MCM-48 and FDU-5,[4] and it is possible to index the calcined XRD pattern (Figure 2d) of AMS-6 on the basis of a cubic *I* lattice with $a = 107.7$ Å. FT diffractograms could be indexed with the incidence beam parallel to the [111] and [110] (Figure 7a and b, respectively) zone axis of a body-centered cubic unit cell with $a = 104.3$ Å. HRTEM images show a high degree of order, and no structural defects could be observed. However, a disordered domain like that of AMS-1 is clearly visible, albeit smaller in thickness. This region has been highlighted in Figure 7a.

AMS-7. The XRD pattern of AMS-7, synthesized with C_{14}-GluSA anionic surfactant and APS as CSDA, is shown in Figure 2e. The synthesis of this material also differs in that tetrapropylammonium bromide (TPABr)

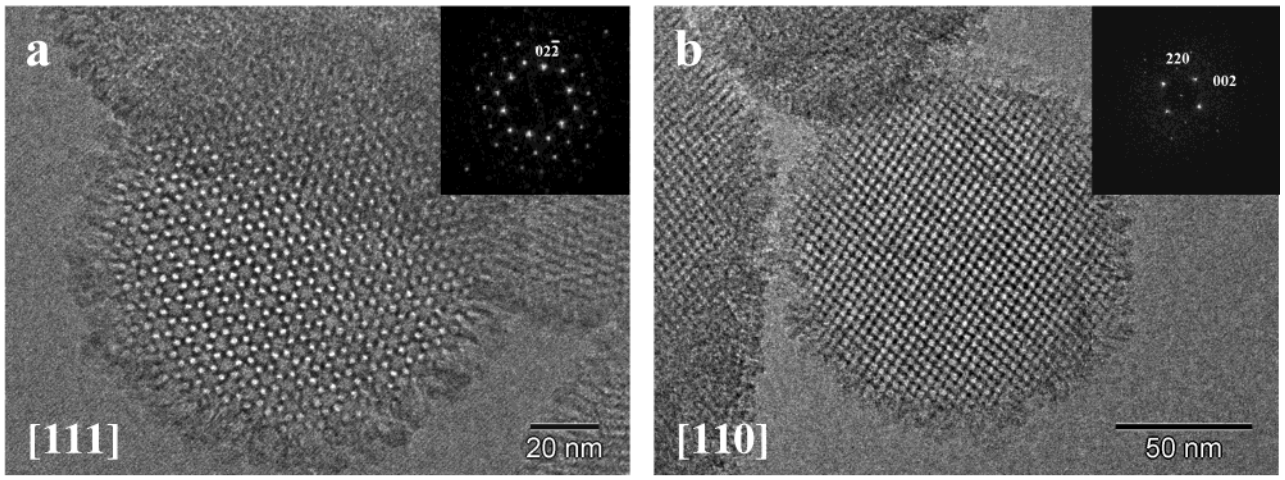

Figure 7. HRTEM images taken along the [111] and [110] orientations of AMS-6. Contrast patterns and FT diffractograms agree with the speculation of a cubic unit cell with $Ia\bar{3}Xd$ symmetry. A cylindrical morphology similar to that of AMS-1 is observed.

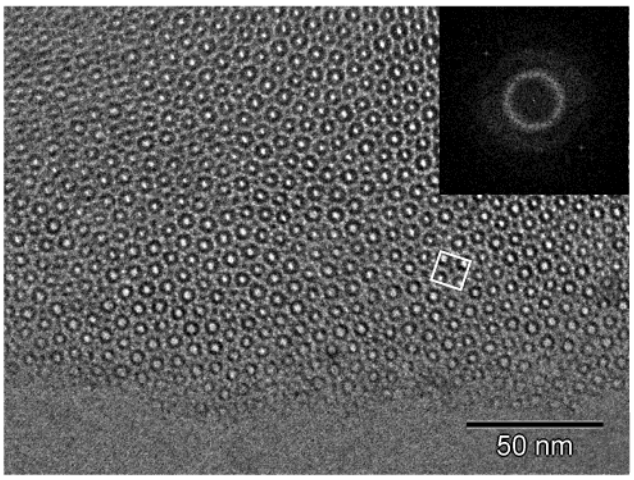

Figure 8. HRTEM image of calcined AMS-7 mesoporous material. The inset shows diffraction rings suggesting that only short-range order can be observed.

was used as an additive. Mesoporous peaks centered between 2 and 5 2θ could be indexed on the basis of a cubic P unit cell with $a = 100.0$ Å. HRTEM images, however, reveal clear modulations in the structure, resembling those described previously for mesoporous material AMS-2. Figure 8 shows a typical HRTEM image recorded with incidence beam parallel to the [100] direction. Short-range periodicity can be observed. In this case modulations are more abundant than in AMS-2 as highlighted by the clean appearance of diffuse diffraction rings in the FT diffractogram.

AMS-8. A series of HRTEM images were recorded along high-symmetry axes of a calcined AMS-8. These are shown in Figure 9a, b, c, and d with the corresponding FT diffractograms shown as insets. All diffraction spots are indexed by a cubic F type structure, unit cell parameter $a = 177.9$ Å. A series of FT diffractograms recorded with different tilt angles along the same particle can be found in the Supporting Information. Figure 9 a, b, and c show images and FT diffractograms recorded along the [121], [233], and [112] orientations of AMS-8, respectively. An image from a different particle oriented along [011] is shown in Figure 9d. All images show a high degree of order. In addition, the clear absence of the $h00$ reflections with $l = 4n + 2$ along the [011] orientation implies the presence of a d glide-plane. This reduces the possible spacegroup symmetry to three types: $Fd\bar{3}$, $Fd\bar{3}m$, and $Fd\bar{3}c$. It is possible to discard $Fd\bar{3}c$ on the basis of observable reflections, which are summarized as $\{hkl$: $h + k$, $h + l$, $k + l$ even$\}$, $\{0kl$: $k + l = 4n$, $k + l$ even$\}$, $\{hhl$: $h + l$ even$\}$, and $\{h00\ h$: $l = 4n$ even$\}$. It is not possible to distinguish between the $Fd\bar{3}$ and $Fd\bar{3}m$ spacegroups, but we can choose the latter on the basis of its higher symmetry. It is worth noting that no stacking faults or evidence of a hexagonal phase were found in AMS-8 suggesting that it is the only 3d-mesophase present in the bulk sample. The XRD pattern of AMS-8 (Figure 2f) can be indexed on the basis of a cubic F unit cell with $a = 183.4$ Å. This value agrees, within experimental error, with the TEM calculated value. Images 9a, b, and c were recorded along the same particle and show a clear domain boundary (highlighted with an arrow on the images). It is possible to suggest that a second phase coexists, but the disordered phase (shown on the top of the image) shows contrast patterns similar to those observed in particles of AMS-1, AMS-2, and AMS-6.

Conclusions

The TEM study here reported shows clearly that the alternative method for the preparation of mesoporous materials using anionic surfactants and aminosilane groups APS and TMAPS as co-structure-directing agents yields highly ordered materials with sharp pore size distributions. It is also worth noting that all materials were stable under the electron beam even after several hours. The presence of 1d-lamellar, 2d-hexagonal, and 3d-cubic/hexagonal structures suggests that this is an improvement of the general synthesis of mesoporous materials, owing to the lower cost of anionic surfactants than cationic or polymeric surfactants. The wide variety of available anionic surfactants and aminosilane groups, and the potential mixtures of these, allow us to envisage the synthesis of new pore connectivities and structures. Indeed, mesoporous material AMS-8 shows TEM contrast patterns and electron diffraction patterns consistent with a 3d-cubic structure with spacegroup $Fd\bar{3}m$. This structure is of great synthetic interest because it remains, to the author's knowledge, unreported using

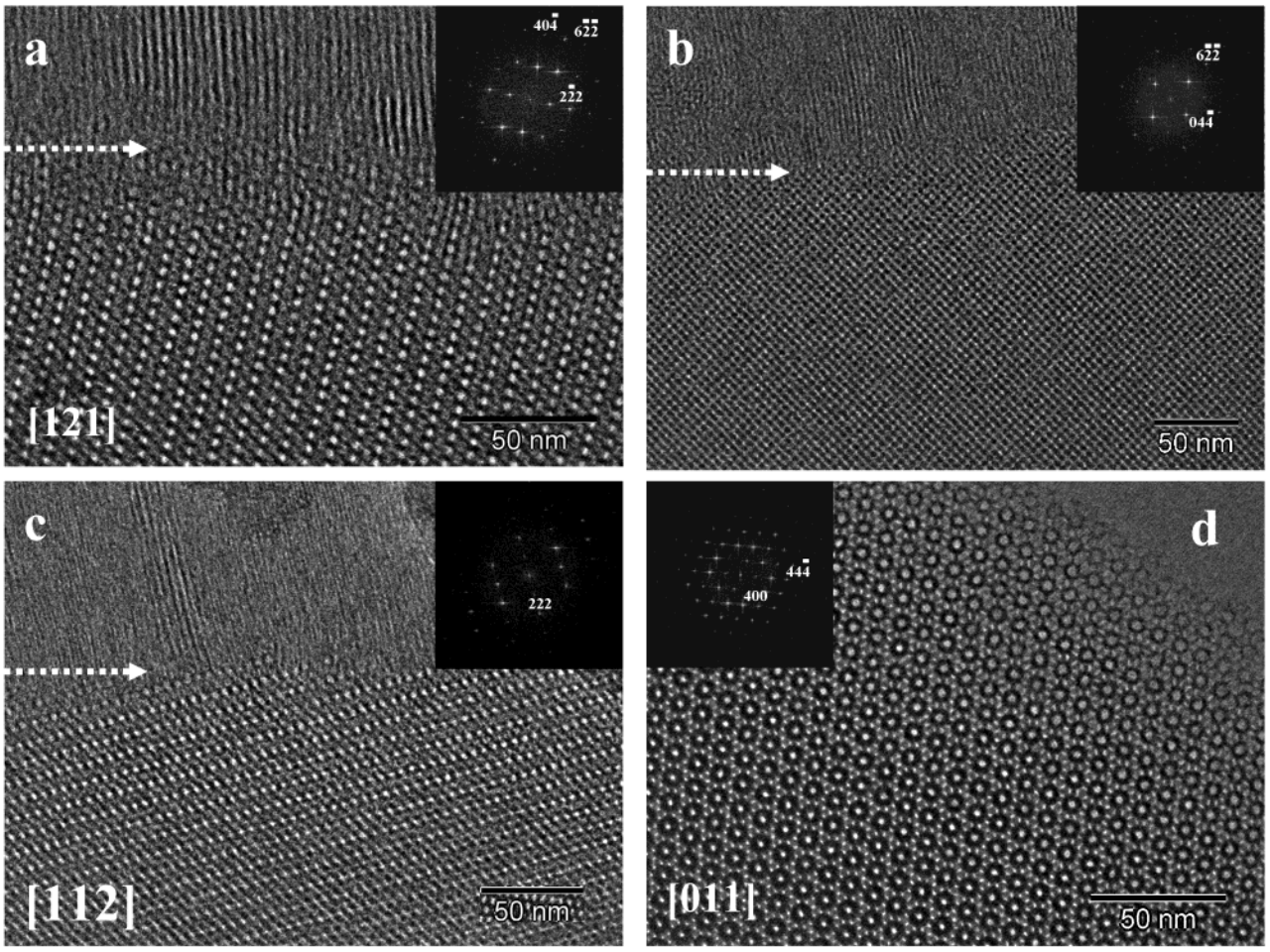

Figure 9. HRTEM image of calcined AMS-8 recorded along the [121], [233], [112], and [011] orientations; (a), (b), and (c) were recorded by tilting along a boundary showing the presence of a 1d disordered domain (highlighted with an arrow). Inset in Figure 9d shows the FT diffractogram taken along a thin area of the image shown. The absence of the 002 reflection and weak intensity of the 006 reflection indicate the presence of a d-glide plane along the [011] direction.

cationic or polymeric surfactants. Further studies are being conducted by means of Fourier 3-d reconstructions to determine the nature of the surface and connectivity of the porous system in AMS-8. A *d*-surface type surface is expected for "diamond" structures. Furthermore, we show clearly the presence of novel structural features such as the evidence of structural modulations, (AMS-2, AMS-7) where the control of these may allow controlling pore connectivity as well as pore shape and size; the growth of a disordered 1-dimensional domain surrounding particles; and a new pore morphology specially suited for catalytic applications, promising faster diffusivity of reactants and products observed for AMS-1 and chiral AMS-6 (analogous with MCM-48). These characteristic features appear to be inherent of the synthetic conditions as well as the use of anionic surfactants and aminosilane groups as co-structure-directing agents. The increased crystallinity of these materials implies the presence of two different types of periodic building units or micelle species.

The necessary synthetic investigations are being conducted to further understand the growth process associated with these materials, as well as to gain an insight into the synthetic mechanism that governs this new method for the preparation of mesoporous materials.

Acknowledgment. We thank Prof. T. Ohsuna and Dr. Y Sakamoto (Arrhenius Laboratory, Stockholm University) for many helpful discussions. AEGB thanks E.U. grant HPRN-CT-2002-00193 for funding. We are grateful to AminoScience Lab, Ajinomoto Co., Inc., for providing *N*-acyl-amino acid and their salt surfactants. This work was partly supported by Core Research for Evolutional Science and Technology (CREST) of JST Corporation to O.T. and T.T.

Supporting Information Available: XRD pattern of calcined AMS-3. FT diffractograms of a tilt series of images recorded along the same particle of calcined AMS-8 mesoporous material (pdf). This material is available free of charge via the Internet at http://pubs.acs.org.

CM035074Z